ARTICLE NO. 78-1459

# Wing Store Active Flutter Suppression—Correlation of Analyses and Wind-Tunnel Data

T.E. Noll* and L.J. Huttsell*
*Air Force Flight Dynamics Laboratory, Wright-Patterson Air Force Base, Ohio*

**Through analyses and recent wind-tunnel tests, active flutter suppression has been shown to be a promising technique for preventing wing/external store flutter restrictions. Data measured in the wind tunnel have been used to evaluate the validity of a method for the design and analysis of active feedback control systems. The results of an analytical effort to study the behavior of an active flutter suppression wind-tunnel model are presented and compared with available test data. For this application, the model was aerodynamically represented by subsonic doublet lattice theory and stability was evaluated using modified Nyquist criteria.**

## Nomenclature

$C$ = control system output
$\bar{c}$ = ratio of control surface chord to corresponding wing chord
$F$ = filter
$\bar{F}$ = characteristic equation
$f$ = frequency, Hz
$G$ = control system forward loop component
$g$ = damping
$H$ = control system feedback loop component
$i$ = $\sqrt{-1}$
$J$ = exponent of the Laplace variable
$K$ = control system gain
$M$ = Mach number
$N$ = modified Nyquist plot encirclements of the origin (+ clockwise)
$P$ = poles of control system characteristic equation
$R$ = control system input
$\bar{R}$ = value of the Nyquist trajectory as it crosses the real axis
$S$ = Laplace variable ($\sigma + i\omega$)
$\bar{s}$ = ratio of control surface span to wing semispan
$V$ = velocity, knots equivalent airspeed
$Z$ = zeros of control system characteristic equation
$\ddot{Z}$ = vertical acceleration, $g$'s
$\delta$ = control surface deflection, deg
$\Lambda$ = sweep angle, deg
$\lambda$ = time constant, s
$\sigma$ = real part of Laplace variable
$\omega$ = frequency, rad/s
$\Delta\bar{G}$ = change in feedback gain required to obtain neutral stability
$\Delta V$ = $(V_{test} - V_{calc})/V_{test}$, %

*Subscripts*

$A$ = auxiliary
$f$ = flutter
$HL$ = hingeline
$m$ = number of zeros in the characteristic equation
$N$ = notch
$n$ = number of poles in the characteristic equation
$S$ = servo
$TE$ = trailing edge
$1,2$ = numerical identification

Presented as Paper 78-1459 at the AIAA Aircraft Systems and Technology Conference, Los Angeles, Calif. Aug. 21-23, 1978; submitted Sept. 20, 1978. 

Index categories: Structural Dynamics; Guidance and Control.

*Aerospace Engineer, Aeroelastic Group, Structures and Dynamics Division. Member AIAA.

## I. Introduction

DURING the last several years, considerable interest has emerged in the application of active control technology to reduce aircraft aeroelastic response. Application of this technology to provide fatigue reduction, gust alleviation, maneuver load control, ride control, and active flutter suppression offers the potential for significant improvements in aircraft performance. For the concept of active flutter suppression, the motion of the lifting surface is sensed and a compensated feedback signal is used to actuate a control surface to damp the critical flutter mode.

Conventional flutter prevention techniques consist of increasing the stiffness, mass balancing, changing geometry, managing fuel distribution, or using speed placards. These solutions generally result in a performance penalty for the aircraft. As a result of the technological base developed for the active control concepts, wing/store flutter suppression is now feasible and provides another option that may be less costly in terms of redesign and reduced operational capability.

This paper presents an analytical study of an active flutter suppression wind-tunnel model which has both a leading-edge control (LEC) and a trailing-edge control (TEC) surface. The paper presents the zero-airspeed frequency response, passive flutter results, and the active flutter suppression analysis results. The analytical results are compared with available ground and wind-tunnel test data.

## II. Discussion

This section presents a description of the active flutter suppression model, a brief discussion of the model wind-tunnel mounting system, and descriptions of the flutter suppression scheme, the analysis concepts, and the aerodynamic representation of the wind-tunnel model.

### Active Flutter Suppression Model Description

Under AFFDL sponsorship, Northrop Corporation designed a wind-tunnel model (Fig. 1) and the active control laws for a wind-tunnel test program to investigate wing/store active flutter suppression.[1] The model was fabricated by Dynamics Technology Inc. The model is a semispan representation of a lightweight fighter (a 30% length scale YF-17 with the exception of the specially designed control surfaces and the addition of an outboard store pylon location). Partial span leading-edge and trailing-edge control surfaces are used as the active flutter suppression surfaces. These

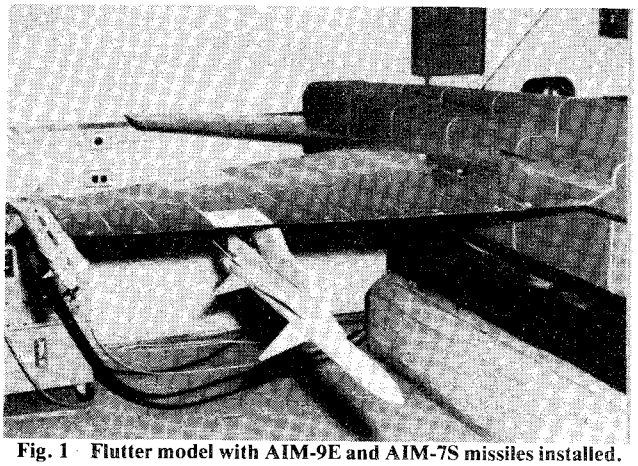

Fig. 1 Flutter model with AIM-9E and AIM-7S missiles installed.

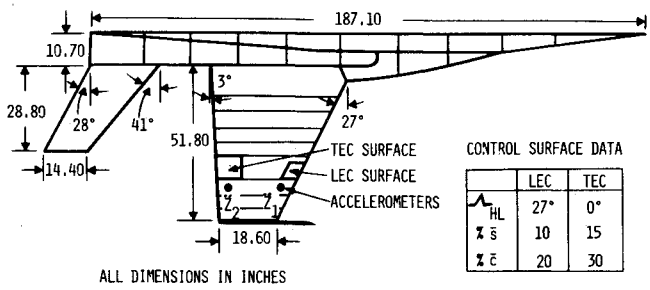


Fig. 2 Wind-tunnel model overall planform dimensions.

control surfaces are driven by miniature hydraulic actuators (fabricated by The Boeing Wichita Company) located near the hingelines. A nondynamically scaled horizontal tail is used to trim the flutter model at various test conditions. The model fuselage is also dynamically scaled; however, the contour is simplified. The model wing has an aluminum spar with ballasted balsa wood sections attached for shape and mass simulation. The wing tip launcher is flexible; however, the pylons were designed to be relatively rigid. The external stores consisted of a rigid AIM-7S, a rigid AIM-9E and a flexible AIM-9E.

A schematic of the model is presented in Fig. 2 and shows overall dimensions. Three different store configurations were selected to simulate symmetric flutter modes with various degrees of violentness (change in damping with respect to a change in velocity at $g=0$) and frequencies. These store configurations are described in Table 1.

### Wind-Tunnel Mounting System

The model was sidewall mounted in the NASA Langley 16-ft Transonic Dynamics Tunnel[2] by a bar-linkage system that permitted the model to move in plunge and pitch, but restrained the model in roll, yaw, and lateral translation. In addition, the model was supported by two fuselage cables to counteract the drag loads. Except for the cable tension and friction of the supporting system, the model simulated symmetric free-free boundary conditions. A splitter plate was installed at the symmetry plane of the fuselage to provide smooth flow over the model. The wind-tunnel tests were conducted in freon at Mach numbers of 0.6 to about 1.1.

### Flutter Suppression Scheme

The control law shown in Fig. 3 illustrates the flutter suppression scheme employed in the tests and this study. Accelerometers located on the wing along a streamwise chord just outboard of the control surfaces (Fig. 2) were used to sense the wing dynamic response. The difference between these two accelerometers (in $g$'s) was fed back through compensation networks to command the oscillation of either the leading-edge or trailing-edge control surface. Figure 3 and Table 2 summarize the compensation used for the three different store configurations. The procedure was to create the proper forces (amplitude, phase, and frequency) with the active control surface to oppose the forces causing flutter and thus stabilize the system. The various filters shown in the block diagram were required to eliminate high-frequency structural modes and to minimize the interaction of the rigid-body modes and the lower-frequency structural vibration modes. The gain and the phase lag were the two key parameters varied during the wind-tunnel test and in the analyses reported herein.

### Analysis Concepts

The structural dynamics data for the model were supplied by the Northrop Corporation in the form of mode shapes, frequencies, and generalized masses for each of the three store configurations. (In generating the structural dynamics data, the horizontal tail and the store pylons were asssumed to be rigid.) The automated flutter analysis module (AFAM) of the FASTOP program[3] was employed to perform the unaugmented flutter calculations. The subsonic doublet lattice[4] option was used to calculate the unsteady aerodynamic force coefficients for two rigid-body modes (plunge and pitch), seven elastic modes, and a control surface rotation mode at six values of reduced velocity (selected to cover the frequency and velocity range of interest). More sets of unsteady aerodynamic force coefficients were needed for the frequency domain flutter suppression analyses. Therefore, 600 sets (600 reduced velocities) were interpolated from the six original sets of aerodynamics.

For the fequency domain analysis, the control system interaction program[5] developed for the earlier active flutter suppression studies[6] sponsored by the AFFDL was used. To determine the augmented aircraft stability characteristics, modified Nyquist criterion was used. Consider the lower portion of Fig. 3. The closed-loop transfer function (output/input) of the system is defined as

$$\frac{C}{R}=\frac{G(S)}{1+G(S)H(S)} \tag{1}$$

where $G(S)$ represents a product of all control system transfer functions in the forward loop, and $H(S)$ represents the product of all control system transfer functions in the feedback loop.

The denominator of Eq. (1) can be defined as $\bar{F}(S)$ and expressed as

$$\bar{F}(S)=\frac{(S+Z_1)(S+Z_2)\cdots(S+Z_m)}{S^J(S+P_1)(S+P_2)\cdots(S+P_n)} \tag{2}$$

Table 1 Description of test configurations

| Configuration | Tip launcher rail | Inboard pylon | Outboard pylon |
|---|---|---|---|
| A | AIM-9E (flexible) | AIM-7S (rigid) | not installed |
| B | empty | not installed | AIM-7S (rigid) |
| C | empty | not installed | AIM-9E (rigid) |

**Table 2 Block diagram transfer functions for each store configuration**

| Element | Configuration A | Configuration B | Configuration C |
|---|---|---|---|
| $F_A$ | $\frac{0.1S}{1+0.02S}$ | $\frac{S}{(1+0.03S)(1+0.015S)}$ | $\frac{S}{(1+0.02S)(1+0.012S)}$ |
| $\lambda$ | 0.0439 | 0.0274 | 0.0108 |
| $K$ | 0.760 | 0.532 | 0.190 |

$$G_S = \begin{cases} \dfrac{3{,}097{,}600\ G_N}{(S+100)(S^2+88S+30{,}976)} & \text{for leading-edge system} \\ \dfrac{1{,}790{,}278\ (S+36)\ G_N}{(S+125)(S+33)(S^2+125S+15{,}600)} & \text{for trailing-edge system} \end{cases}$$

$$G_N = \frac{S^2+21S+45{,}590}{S^2+299S+45{,}590}$$

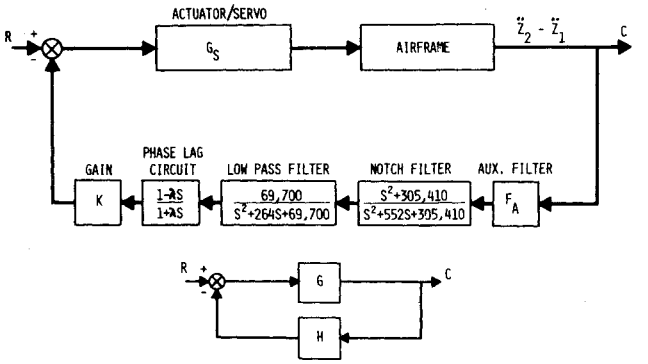


**Fig. 3 Active flutter suppression block diagram.**

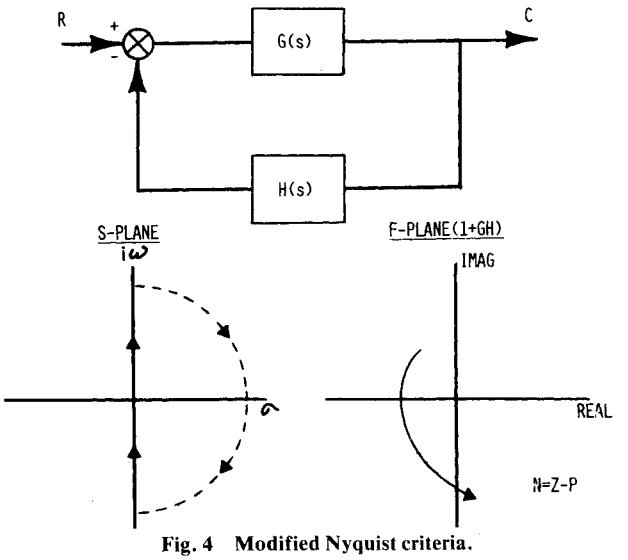


**Fig. 4 Modified Nyquist criteria.**

When $\bar{F}(S)$ is set equal to zero, the resulting expression is called the characteristic equation of the system. The zeros of $\bar{F}(S)$ are defined as the roots of the characteristic equation and can be real, pure imaginary, or complex numbers. For a stable closed-loop system, all of the roots (zeros) of $\bar{F}(S)$ must have negative real parts. There is no particular restriction on the poles of $\bar{F}(S)$; however, it is of interest to note that the poles of $\bar{F}(S)$ are also the poles of $G(S)\,H(S)$, which is defined as the open-loop system. If any of the poles of $G(S)\,H(S)$ lie in the right half of the $S$ plane (positive real parts) the open-loop transfer function will be unstable. The closed-loop system, however, can still be stable if all the zeros of $\bar{F}(S)$ are found in the left half of the $S$ plane. The $S$ plane as referred to herein is a plot of the zeros and poles of $\bar{F}(S)$ in the complex plane.

The objective of the modified Nyquist theory is to determine if any of the roots of the characteristic equation $[\bar{F}(S)=0]$ lie in the right half of the $S$ plane. The approach (Fig. 4) is to define a trace (Nyquist path) that encircles the entire right half of the $S$ plane and that encloses all the poles and zeros of $\bar{F}(S)$ which may lie in the right half of the $S$ plane. Once this trace is specified, the stability of the closed-loop system can be determined by plotting $\bar{F}(S)$ as $S$ takes on values along the trace, and investigating the behavior of the $\bar{F}(S)$ plot with respect to the origin of the $\bar{F}$ plane. The $\bar{F}(S)$ locus mapped into the $\bar{F}$ plane will encircle the origin as many times as the difference between the number of zeros and the number of poles of $\bar{F}(S)$ that were encircled by the trace. In other words,

$$N=Z-P \tag{3}$$

where

$N=$ the number of encirclements of the origin made by the $\bar{F}(S)$ locus in the $\bar{F}$ plane

$Z=$ number of zeros of $\bar{F}(S)$ on the right-hand side of the $S$ plane

$P=$ number of poles of $\bar{F}(S)$ on the right-hand side of the $S$ plane

For a stable system, $Z$ must always be zero, which implies that the Nyquist plot of $\bar{F}(S)$ must encircle the origin $P$ times. The encirclements, if any, must be made in a negative (counterclockwise, $N=-P$) direction, since the Nyquist path in the $S$ plane was assumed in the clockwise direction. If the aircraft speed is below flutter onset, there are no poles in the function $G(S)$. There are also no poles of $H(S)$ in the right half of the $S$ plane as can be determined from inspection. Therefore, for this case, $P=0$. As a result, any clockwise encirclement of the origin indicates an instability. If the aircraft is above the flutter speed, there will be a pole(s) in the right half of the $S$ plane; therefore, there must be a counterclockwise encirclement for each pole for the system to be stable. The frequency of the critical mode (flutter mode) can be found by locating the point at which $\bar{F}(S)$ crosses the real axis (the value of frequency required to cause $\bar{F}(S)$ to be real). The change in gain required (in dB) to obtain neutral stability has

been derived as

$$\Delta\bar{G} = 20 \log \left| \frac{1}{\bar{R}-1} \right| \tag{4}$$

where $\bar{R}$ is the value of $\bar{F}(S)$ as it crosses the real axis [ in the range from $(+1,0)$ coordinate to $(-\infty,0)$]. The phase margin (in deg) is defined as the rotation of $\bar{F}(S)$ about the $(+1,0)$ coordinate, in a positive or negative sense, necessary to cause $\bar{F}(S)$ to encircle the origin.

#### Aerodynamic Representation

As previously mentioned, the subsonic doublet lattice method was used to calculate the unsteady aerodynamic forces on the model. The doublet lattice representation used for this study is shown in Fig. 5. The model was divided into 17 aerodynamic panels (one for the wing leading-edge extension, eight for the wing, one for the tip missile/launcher, two for the horizontal tail, and five for the fuselage interference panels). The panels were further subdivided into aerodynamic boxes. There were four boxes on the wing leading-edge extension, 88 boxes on the wing (including eight boxes on the leading-edge control surface and 12 boxes on the trailing-edge control surface), 10 on the missile/launcher, 27 on the horizontal tail, and 40 on the fuselage interference panels for a total of 169 boxes. The aerodynamic effects of the 5-deg wing anhedral and the horizontal tail offset from the fuselage centerline were taken into account. In this analysis, it was assumed that the aerodynamic interference between the store/pylon and the wing was negligible. The tip missile and launcher were represented aerodynamically as flat plates.

## III. Results

In this section, the results of various stages of the analysis are presented and compared with available test data.[1,7] Results are shown for the zero airspeed calculations for the airframe dynamics (servoelastic); flutter analyses with the system off (aeroelastic); and frequency domain analyses with the system operating (aeroservoelastic).

#### Zero Airspeed Results

The accuracy of the analytical representation of the model dynamics was investigated by calculating zero airspeed frequency response data at selected sensor locations for either a leading-edge or trailing-edge control input. A comparison of calculated and measured zero airspeed frequency response data for the forward loop ($G$ as shown in the lower part of Fig. 3) is provided in Fig. 6. The forward loop consists of the actuator/servo and the airframe dynamic characteristics. The example shown is for configuration A. An acceleration ($\ddot{Z}_2$) was measured during the test for a trailing-edge control surface input. Only the wing modes used in the flutter suppression analyses are identified on the figure. The test data are presented as a solid line with the test frequencies shown in parentheses. In terms of amplitude ratio, the comparisons of peak values for the modes of interest between analysis and test data agreed very well. There were two additional measured modes shown on the figure around 17 and 21 Hz which were not represented in the analyses; these modes were pylon and horizontal tail bending modes, respectively. As stated previously, the pylon and the tail were assumed rigid in the analytical representation of the wind-tunnel model. Similar data were obtained for other sensor locations for both the leading-edge and trailing-edge control surfaces and for each of the three store configurations. The resulting comparisons were similar to those presented for configuration A.

#### Unaugmented Flutter Results

Unaugmented flutter analyses (active system off) were conducted for each of the three store configurations at the test Mach numbers using the FASTOP P-k option. The calculated flutter speeds presented in this paper do not represent matched point conditions, i.e., the assumed Mach number and air density do not correspond to the flutter speed. This approximation should not significantly affect the results presented. Figures 7 and 8 present typical results for one of the store configurations. These figures show velocity vs damping and velocity vs frequency trends for configuration B at a Mach number of 0.8. The flutter mechanism primarily involved coupling of modes 3 and 4 (wing first bending and torsion modes). Flutter was predicted at a speed of 150 KEAS (knots equivalent airspeed) at 6.7 Hz assuming zero structural damping. This was 4.5% conservative when compared with test data. For configuration A, the calculated flutter mode was a very mild "hump mode" with the maximum positive damping not exceeding 0.059. For zero structural damping, flutter was predicted at a velocity of 203 KEAS at 12.4 Hz; for 2% structural damping the flutter speed increased to about 230 KEAS and the frequency dropped slightly. During the wind-tunnel test, configuration A did not flutter due to the

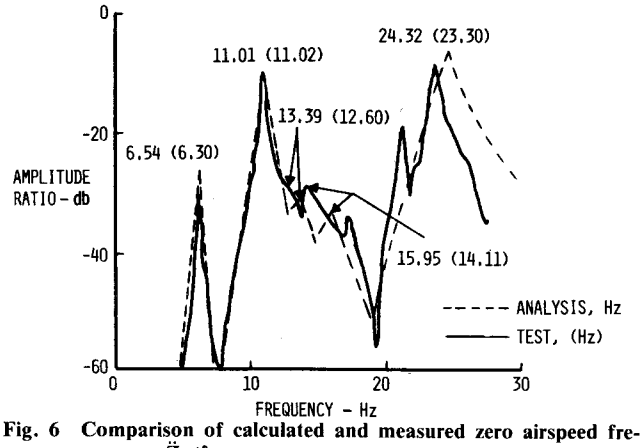


**Fig. 6 Comparison of calculated and measured zero airspeed frequency response, $\ddot{Z}_2/\delta_{TE}$.**

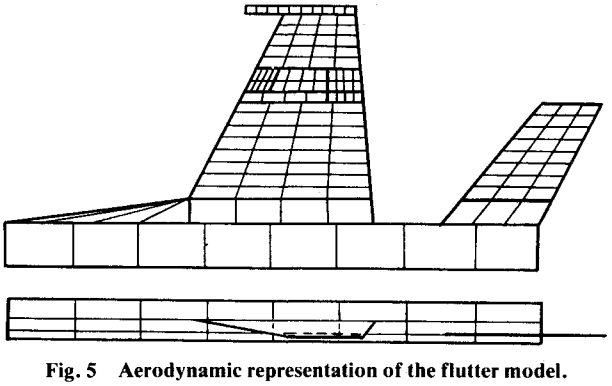

**Fig. 5 Aerodynamic representation of the flutter model.**

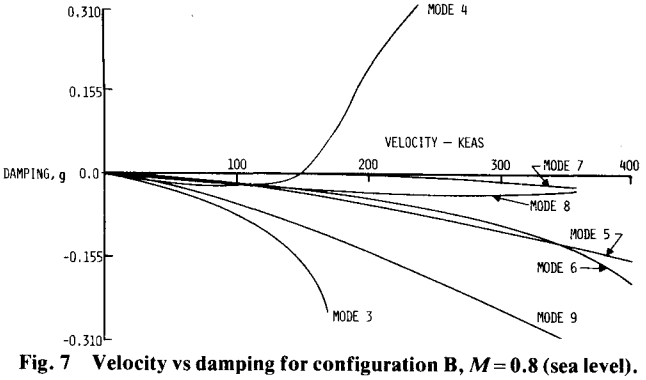


**Fig. 7 Velocity vs damping for configuration B, $M = 0.8$ (sea level).**

unexpectedly high damping attributed to the model support system. The results of the passive flutter analyses are summarized in Table 3 along with augmented calculations which will be discussed in the next section.

Table 3 also summarizes the unaugmented flutter results when ground vibration test (GVT) data[8] were included in the analyses. These results are shown in parentheses. For configuration A, flutter was predicted at 201 KEAS when the GVT modes and frequencies were used. This can be compared to 203 KEAS, the calculated flutter speed when analytical modes were used. For configuration B, flutter was predicted at 159 KEAS when the GVT data were used; this was 1.3% unconservative when compared to the test data. Configuration C was predicted to flutter at 174 KEAS with the calculated modes and 151 KEAS when GVT data were used. This was 1.1% and 14.2% conservative when compared to the test data, respectively. All of the calculated data shown in the table were for zero percent structural damping.

#### Active Flutter Suppression Results

The active flutter suppression analyses were conducted in the frequency domain using calculated modal characteristics and modified Nyquist criteria as discussed. Figures 9-14 present the results of the flutter suppression analyses and provide comparisons between the calculated and test data for each of the three external store configurations. Table 3 summarizes the analyses and test data with the active system on and off for each store configuration.

The results for configuration A are presented in Figs. 9 and 10. Figure 9 shows modified Nyquist plots for increasing airspeed. The active surface in this case was the trailing-edge control surface. Passive flutter was predicted to occur at a velocity of approximately 203 KEAS. At speeds below the passive flutter condition, the Nyquist plot for the critical mode (flutter mode) formed a clockwise loop for increasing frequencies. As the speed approached the flutter velocity, the Nyquist plot grew in response but continued to form a loop in the clockwise direction. At flutter, the Nyquist plot near the flutter mode frequency approached a straight line (loop of infinite radius). At a speed increment slightly above flutter, the Nyquist plot had a counterclockwise encirclement of the origin. Since a flutter condition is represented by a pole in the right half plane of the $S$ domain, Nyquist criteria require the plot to encircle the origin in a counterclockwise direction to be stable. If the plot does not, the aircraft is unstable in the flutter mode. As the speed was increased, the Nyquist plot tended to get smaller or began to rotate about the $(+1,0)$ point until the loop no longer encircled the origin. This characteristic change in the Nyquist plot was not as noticeable for configuration A as it was for configuration B and C (shown later in Figs. 11 and 13). Configuration A would be stable to speeds significantly higher than 240 KEAS with the system operating. The improvement in flutter speed would be greater than 18%. Figure 10 shows the experimental results with the trailing-edge flutter suppression system on and off. As mentioned earlier, configuration A did not flutter in the tunnel. However, it can be seen from the test data that the trailing-edge system added significant damping to the critical mode.

Figures 11 and 12 show similar calculated and test results for configuration B for a Mach number of 0.8. Figure 11

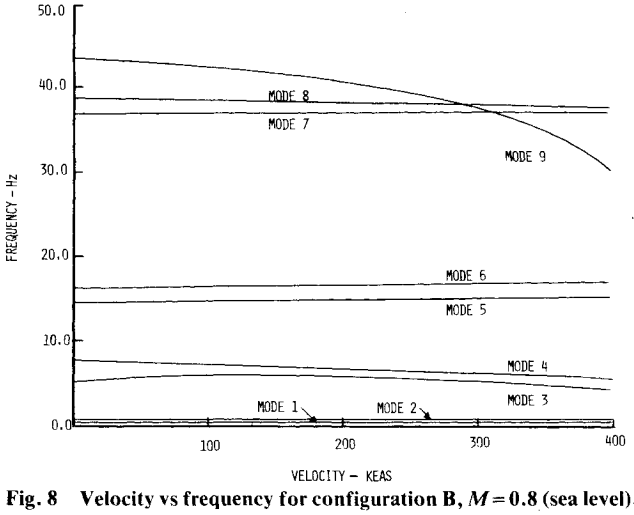


**Fig. 8 Velocity vs frequency for configuration B, $M = 0.8$ (sea level).**

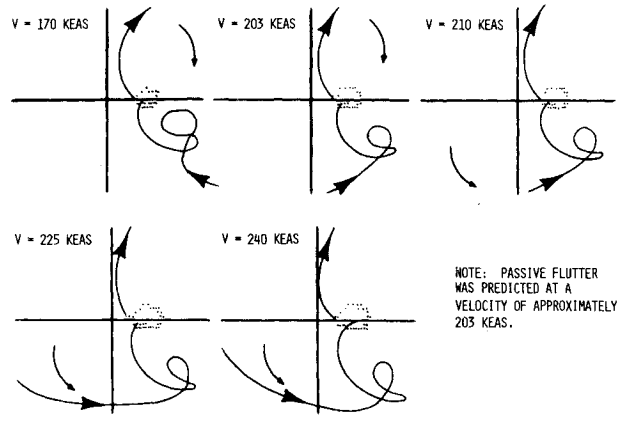


**Fig. 9 Modified Nyquist plots for configuration A, trailing-edge control law, $M = 0.8$ (sea level).**

**Table 3 Summary of comparisons between calculated and test results[a]**

| | Unaugmented results | | | | | Augmented results | | | | |
|---|---|---|---|---|---|---|---|---|---|---|
| | Test | | Calculated | | | Test | | Calculated | | |
| Configuration | $V$,KEAS | $f$,Hz | $V$,KEAS | $f$,Hz | $\Delta V$% | $V$,KEAS | $f$,Hz | $V$,KEAS | $f$,Hz | $\Delta V$% |
| A | | | | | | | | | | |
| $M=0.8$ | no flutter $V_f > 221$ | | 203 | 12.4 | ··· | $V_f > 221$ | | $V_f > 240$ | | ··· |
| Trailing-edge control law | | | (201)[c] | (12.1) | ··· | | | | | |
| B | | | | | | | | | | |
| $M=0.8$ | 157 | 5.8 | 150 | 6.7 | 4.5 | 171[b] | ··· | 179 | 6.7 | −4.7 |
| Leading-edge control law | | | (159) | (6.3) | −1.3 | | | | | |
| C | | | | | | | | | | |
| $M=0.6$ | 176[b] | 8.4 | 174 | 10.4 | 1.1 | 193[b] | ··· | 219 | 10.4 | −13.5 |
| Leading edge control law | | | (151) | (9.3) | 14.2 | | | | | |

[a] All results at $g = 0$. [b] Extrapolated from test data. [c] ( ) = Calculated using GVT mode shapes and frequencies.

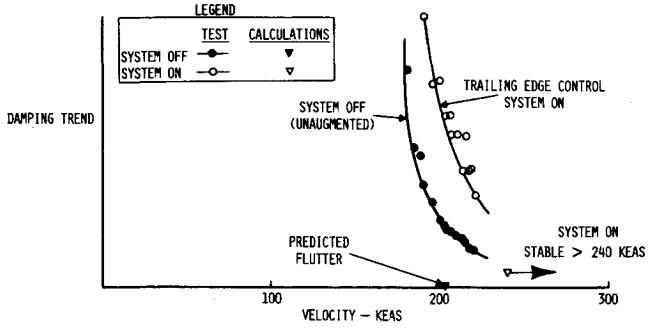


**Fig. 10 Comparison of calculated and test results for configuration A, $M = 0.8$.**

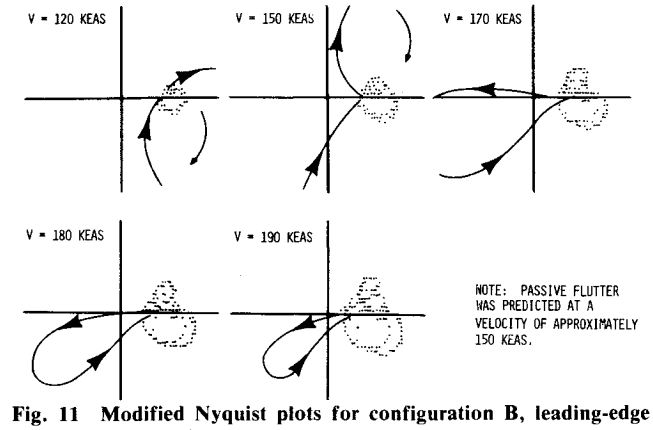


**Fig. 11 Modified Nyquist plots for configuration B, leading-edge control law, $M = 0.8$ (sea level).**

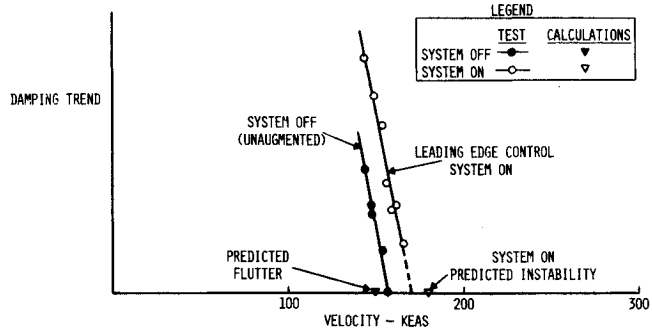


**Fig. 12 Comparison of calculated and test results for configuration B, $M = 0.8$.**

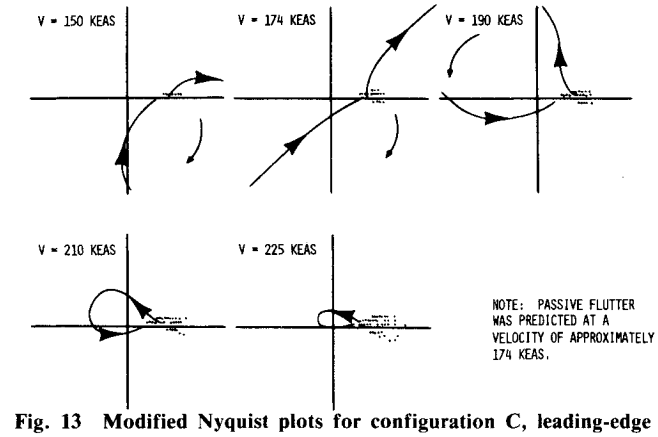


**Fig. 13 Modified Nyquist plots for configuration C, leading-edge control law, $M = 0.6$ (sea level).**

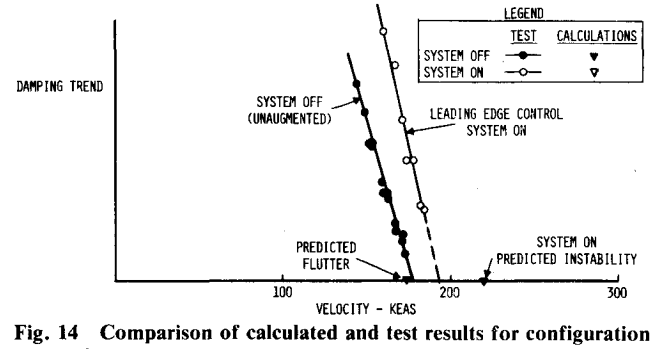


**Fig. 14 Comparison of calculated and test results for configuration C, $M = 0.6$.**

shows the Nyquist plot variation with airspeed for the active leading-edge control system. For this configuration, flutter was predicted to occur at 150 KEAS. For this case, the critical loop of the Nyquist plot tended to rotate in a counterclockwise direction about the (+1,0) point as the model speed was increased. With additional phase lag (30 deg at approximately 6 Hz) in the control law, the augmented flutter speed could be further increased. However, the critical loop became quite narrow, which would indicate very low phase margins. For the leading-edge control law analyzed, the flutter speed improvement was predicted to be about 19%. Figure 12 shows test data plotted vs airspeed for both system on and off. From the test data, the projected augmented flutter speed was 171 KEAS. Therefore, the test data showed a flutter speed improvement of approximately 9%. The predicted system-on instability (179 KEAS) was 4.7% higher than the similar condition projected from test data (171 KEAS).

The analysis and test data for configuration C at a Mach number of 0.6 are presented in Figs. 13 and 14. Figure 13 presents the Nyquist plot variation with airspeed for the leading-edge control system. Flutter, in this case, was predicted to occur at a speed of 174 KEAS. The trend of the shape of the critical loop of the Nyquist path with airspeed very closely followed the classical description presented earlier. At flutter (upper middle plot), the loop appeared to approach a straight line. It is also interesting to note that in this case, the Nyquist plot rotated in a clockwise direction about the (+1,0) point with increasing airspeed. This was contrary to the results presented for configuration B (Fig. 11). It would be beneficial in this case, in terms of increased flutter speed, if about 15-deg phase lead at 10 Hz were added to the control law. Once again, the model would be stable for speeds exceeding 225 KEAS but with very low gain and phase margins. Figure 14 presents the test results for configuration C with the active leading-edge control law. The projected system-off and system-on instabilities from test data were 176 KEAS and 193 KEAS, respectively. This was about a 10% increase in flutter speed. The analyses predicted passive flutter at 174 KEAS and augmented flutter at 219 KEAS for an increase in flutter speed of 26%.

In general, control surface aerodynamic and moment coefficients predicted by theory are high when compared to experimental data. Since experimental control surface aerodynamics were not available for this model, there was no attempt in this study to reduce the magnitude of the control surface aerodynamics. Unmodified control surface aerodynamics tend to predict a more efficient active flutter suppression system. This may be a partial explanation of the differences obtained between the analysis and test results with the active flutter suppression system-on.

## IV. Concluding Remarks

This paper presents the results of an analytical study of a wing/store active flutter suppression wind-tunnel model. Three different external store configurations were analyzed. Both a leading-edge and a trailing-edge control surface acting alone were used in the analysis as the active flutter sup-

pression aerodynamic force producer. Unsteady doublet lattice aerodynamics were calculated and used in conjunction with modified Nyquist criteria to provide stability evaluation. The control laws which were found to be most effective during the wind-tunnel tests were analyzed, and the resulting speed improvements were compared with available test data. In all cases, the predicted passive flutter speed for each store configuration using calculated mode characteristics was conservative when compared to test data. When similar calculations were made using ground vibration test data, the resulting passive flutter speed predictions varied from slightly unconservative (configuration B) to conservative (configurations A and C). Calculation with the active flutter suppression system operating indicated a larger flutter speed improvement than the projected test data showed. This was expected because of the use of unmodified control surface aerodynamics in the analysis procedure.

This paper has shown that Nyquist stability criteria are a valuable tool for the design and analysis of active flutter suppression systems. However, care must be taken to assure that the aerodynamics, the structural dynamics and the control system representations of the aircraft are well defined through comparisons with available experimental data.

The Air Force has plans to continue testing the flutter model described herein to investigate improved single surface control laws and control laws which use both the leading-edge and trailing-edge control surfaces acting together. The most challenging aspect of wing/store flutter suppression appears to be automatic adaptive control. Since other store configurations can result in different flutter modes of widely varying characteristics, the feedback compensation required to suppress the flutter mode of each store configuration must be variable. The objective of adaptive control is to obtain sufficient information (i.e., flight conditions, store configurations, etc.) that would be necessary to provide in an efficient manner the feedback compensation required for flutter prevention. Plans are to investigate further adaptive control devices with the objective of implementing the most promising technique for demonstration in the wind tunnel. Also, additional work is required to improve and evaluate unsteady aerodynamic methods for oscillating control surfaces.

## References

[1] Hwang, C., Winther, B.A., and Mills, G.R., "Demonstration of Active Wing/Store Flutter Suppression Systems," Air Force Flight Dynamics Laboratory, Wright-Patterson Air Force Base, Ohio, AFFDL-TR-78-65, June, 1978.

[2] Staff of the Aeroelasticity Branch, "The Langley Transonic Dynamics Tunnel," NASA LWP 799, Sept. 1969.

[3] Wilkinson, et al, "An Automated Procedure for Flutter and Strength Analysis and Optimization of Aerospace Vehicles," Air Force Flight Dynamics Laboratory, Wright-Patterson Air Force Base, Ohio, AFFDL-TR-75-137, Vols. I and II, Dec. 1975.

[4] Giesing, J.P., Kalman, T.P., and Rodden, W.P., "Subsonic Unsteady Aerodynamics for General Configurations," Air Force Flight Dynamics Laboratory, Wright-Patterson Air Force Base, Ohio, AFFDL-TR-71-5, Pt. 1, Vols. I and II, Nov. 1971.

[5] Noll, T.E. and Huttsell, L.J., "Control System/Airframe Interaction Analyses for the YF-16 Missile-On Configuration," Air Force Flight Dynamics Laboratory, Wright-Patterson Air Force Base, Ohio, AFFDL-TM-77-3-FBR, March 1977.

[6] Triplett, W.E., Kappus, Hans-Peter F., and Landy, R.J., "Active Flutter Suppression Systems for Military Aircraft, a Feasibility Study," Air Force Flight Dynamics Laboratory, Wright-Patterson Air Force Base, Ohio, AFFDL-TR-72-116, Feb. 1973.

[7] Hwang, C., Winther, B.A., Noll, T.E., and Farmer, M.G., "Demonstration of Aircraft Wing/Store Flutter Suppression Systems," *AGARD Structural Dynamics and Materials Panel,* April 1978.

[8] Voelker, L.S., "Ground Vibration Test of the Active Flutter Suppression Transonic Model with External Stores," Air Force Flight Dynamics Laboratory, Wright-Patterson Air Force Base, Ohio, AFFDL-TM-77-92, Dec. 1977.